The Journal of Chemical Physics

RESEARCH ARTICLE | NOVEMBER 27 2018

Electron attachment to hexafluoropropylene oxide (HFPO)

M. Zawadzki; A. Chachereau; J. Kočišek; C. M. Franck; J. Fedor

J. Chem. Phys. 149, 204305 (2018)
https://doi.org/10.1063/1.5051724

Electron attachment to hexafluoropropylene oxide (HFPO)

M. Zawadzki,[1,2] A. Chachereau,[3] J. Kočišek,[1] C. M. Franck,[3,a)] and J. Fedor[1,a)]
[1]*J. Heyrovský Institute of Physical Chemistry, Czech Academy of Sciences, Dolejškova 3, 18223 Prague, Czech Republic*
[2]*Department of Atomic, Molecular and Optical Physics, Faculty of Applied Physics and Mathematics, Gdańsk University of Technology, ul. G. Narutowicza 11/12, 80-233 Gdańsk, Poland*
[3]*Power Systems and High Voltage Laboratories, ETH Zurich, Physikstr. 3, 8092 Zurich, Switzerland*

(Received 11 August 2018; accepted 26 October 2018; published online 27 November 2018)

We probe the electron attachment in hexafluoropropylene oxide (HFPO), C_3F_6O, a gas widely used in plasma technologies. We determine the absolute electron attachment cross section using two completely different experimental approaches: (i) a crossed-beam experiment at single collision conditions (local pressures of 5×10^{-4} mbar) and (ii) a pulsed Townsend experiment at pressures of 20–100 mbar. In the latter method, the cross sections are unfolded from the electron attachment rate coefficients. The cross sections derived independently by the two methods are in very good agreement. We additionally discuss the dissociative electron attachment fragmentation patterns and their role in the radical production in industrial HFPO plasmas. *Published by AIP Publishing.*
https://doi.org/10.1063/1.5051724

I. INTRODUCTION

HFPO (hexafluoropropylene oxide, C_3F_6O, structure shown in Fig. 2) is a gas that is commonly used as a fluorointermediate in the organic synthesis of fluoromonomers and fluoropolymers and to add fluorine functionality to a variety of organic precursors.[1] A part of the reason for its success in fluoropolymer chemistry is the fact that it contains a strained epoxide ring. This ring is relatively easy to open by various chemical pathways which induce polymerization. Due to the strain, HFPO also decomposes thermally at relatively low temperatures.[2]

HFPO has thus been increasingly used as a precursor in the plasma-assisted polymerization, especially to produce low dielectric constant fluorocarbon thin films.[3] Such films have polytetrafluoroethylene (PTFE)-like ($[CF_2]_n$) structure and have a variety of technological applications, e.g., liquid repellency, insulating electronic materials, encapsulation barrier layers, and biologically implantable devices.[4] Interestingly, more efficient polymerization is achieved by the use of time-modulated glow discharges:[5] lowering the duty cycle results in a progressively less branched polymeric film structure with higher F/C ratio, which is more similar to polytetrafluoroethylene (PTFE). This has been ascribed primarily to changes of the plasma chemistry during the off phase, especially due to changes in the concentration of the CF_2 radical transient.[3,6] Since the CF_2 radical is readily formed upon the thermal decomposition,[2] it has been speculated that it is also a dominant product of the electron-induced chemistry in plasmas.[3,4,6]

A further source of interest in HFPO is its potential use as an electric insulation gas. Since it is a fully fluorinated gas, it is likely to be strongly electron attaching. HFPO has a boiling point of −28° C and its vapor pressure at 0° C is 0.3 MPa.[7] Therefore, pure HFPO or HFPO mixtures with a suitable buffer gas could prove interesting as electrical insulation media. Currently, SF_6 is widely used in medium and high voltage insulation applications, but it has a high global warming potential (GWP). The 100-year integrated GWP of SF_6 is about 23 500.[8] The GWP of pure C_3F_6O is estimated to be about a quarter of that, namely, 6200,[9] based on a radiative forcing of 0.260 Wm^{-2} ppb^{-1} and an atmospheric lifetime of 90 years with respect to reactivity with OH radicals. The actual atmospheric lifetime of HFPO might be much shorter considering reactivity with other compounds[10] or UV photolysis. Another source claims that HFPO's atmospheric lifetime is shorter than 10 years,[11] which would bring its GWP below 1000.

From these points of view, it is somewhat surprising that neither the electron-impact fragmentation patterns nor the electron collision cross sections are known for this gas. As to the plasma chemistry, due to the high electron affinity of fluorine, it is reasonable to assume that the negative ion fragmentation via dissociative electron attachment (DEA) will play an important role in the production of radicals. It is, however, well known that the electron-induced decomposition pathways may be very different from the thermochemical ones and the cross sections for individual fragmentation channels strongly depend on the position and width of the involved transient anion states. As to the dielectric applications, the electron attachment cross section is one of the crucial properties in determining breakdown properties.

There are two major possible approaches of experimentally addressing the electron attachment cross sections. The first one is to probe the electron-molecule interactions in a *beam experiment* at single collision conditions, where the environment does not interfere with the reaction. The second one

a)Electronic addresses: juraj.fedor@jh-inst.cas.cz and cfranck@ethz.ch

is to send an electron pulse trough a higher-pressure sample (often diluted in a buffer gas) in a *swarm experiment* and measure the transport parameters. These two approaches often lead to different results[12–14] caused by the three-body processes in the higher-pressure environment.

In the present work, we probe electron attachment to HFPO with the two methods. In this case, they yield very good agreement. We discuss the molecular origins of this fact and put them in context of the fragmentation pattern and dynamics in the resonant collisions of this gas with free electrons.

II. EXPERIMENT

Two different approaches were taken.

A. Beam experiment (Prague)

In the first approach, electron attachment to HFPO is probed at single-collision conditions using two different experimental setups.

The first setup is a quantitative electron attachment spectrometer with a time-of-flight mass analyzer.[15,16] A pulsed electron beam produced in a trochoidal electron monochromator passes a collision cell filled with a stagnant target gas at a pressure of 1 - 5 × 10^{-4} mbars. The created anions are extracted perpendicularly to the electron path into the mass analyzer. The collision cell, ion optics, and the ion detection scheme were designed such that the extraction, transmission, and the detection efficiency are independent of the ion mass or initial kinetic energy.[16] The cross sections are normalized against a well-known cross section for the production of O^- from CO_2 at the 4.4 eV band[17] (integrated cross section of 13.3 eV pm^2).

The second setup is a dissociative electron attachment spectrometer with a quadrupole mass filter.[18] The continuous electron beam from the trochoidal electron monochromator crosses the effusive beam of the target gas. The anions are mass analyzed in the quadrupole, placed perpendicularly to the electron and molecular beams.

The electron energy scale in both setups is calibrated using the 4.4 eV resonance in CO_2. The presence of low-energy electron in the incident beam is verified by recording the SF_6^- ion yield from SF_6 which reaches very high values close to 0 eV. The time-of-flight setup produces electrons with energies down to roughly 100 meV, and the quadrupole setup to roughly 50 meV. Due to the absence of the pulsing, the second setup has better electron energy resolution than the first setup (100 meV vs. 250 meV). The final beam partial cross sections are thus obtained by scaling the ion-yield curves from the quadrupole apparatus to the absolute data from the TOF apparatus using the invariance of the energy-integrated cross section.

B. Swarm experiment (Zürich)

In the second approach, the effective ionization rate coefficient, electron drift velocity, and diffusion coefficient of HFPO are investigated in the pulsed Townsend setup described by Dahl *et al.*[19] The HFPO sample used in the swarm experiment has a purity of 99% (SynQuest Labs), the N_2 a purity of 6.0, and the CO_2 a purity of 5.0. The mixtures of HFPO with N_2 and CO_2 are filled into the gas vessel previously evacuated to a pressure of ~0.1 Pa. A short laser pulse (1.5 ns FWHM) releases about 10^7 electrons from a back-illuminated palladium thin-film photocathode. The electron swarm drifts in a uniform electric field between two Rogowski shaped electrodes. The electrode spacing is varied from 13 to 19 mm and the applied voltage from 50 V to 5 kV. The measurements are performed at room temperature and in the pressure range of 2–10 kPa. The swarm parameters depend on the reduced field strength E/N, given in townsend (1 Td = 10^{-21} Vm^2), where E is the electrical field strength and N is the number density of the gas. The displacement current I_{exp} of the charged particle swarm drifting in the gap is measured.

The measured current I_{exp} is the sum of the electron and ion currents I_e and I_{ion}. These two components are separated using an iterative procedure.[20] The electron current I_e can be expressed analytically for $t \geq 0$ as[19,20]

$$I_e(t) = \frac{I_0}{2} e^{k_{eff} N t} \left(1 - \mathrm{erf}\left(\frac{t - T_e}{\sqrt{2\tau_D t}}\right)\right), \quad (1)$$

$$I_0 = \frac{N_e(0) q_0}{T_e}, \quad (2)$$

where I_0 is the electron current at time $t = 0$, k_{eff} is the effective ionization rate coefficient, N is the number density of the gas, T_e is the electron drift time, which relates to the bulk electron drift velocity w_e via $T_e = d/w_e$, τ_D is the characteristic time for longitudinal electron diffusion, which relates to the longitudinal diffusion coefficient ND_L via $2ND_L = w_e^2 N \tau_D$, $N_e(0)$ is the initial number of electrons, and q_0 is the elementary charge.

The measured electron current I_e is fitted[20] with Eq. (1) to obtain the effective ionization rate coefficient k_{eff}, the electron drift velocity w_e, and the longitudinal electron diffusion coefficient ND_L. The effective ionization rate coefficient k_{eff} is equal to the difference between the ionization and attachment rate coefficients, $k_{eff} = k_i - k_a$. Sample measurements and fits of the electron current are shown in Fig. 1. According to Eq. (1), an exponential decrease of the current corresponds to a negative value of the effective ionization rate coefficient k_{eff}, which means that electron attachment dominates over impact ionization: $k_a > k_i$.

The overall electron attachment cross section of C_3F_6O is then derived from the measured values of k_{eff} using a linear inversion method.[21] This method gives an estimation of the attachment cross section of a strongly electron-attaching gas by using swarm measurements where the electron-attaching gas is mixed in small proportions to various buffer gases. In this case, the relation between k_{eff} and the attachment cross section σ_a is given by

$$k_{eff}(E/N) = (1 - x)\, k_{eff}^b(E/N) + x\sqrt{\frac{2}{m_e}} \int_0^\infty \sigma_a(\varepsilon)\, \varepsilon\, f(E/N, \varepsilon)\, \mathrm{d}\varepsilon. \quad (3)$$

Here k_{eff} is the effective ionization rate coefficient in the gas mixture containing a mole fraction x of the electron-attaching gas, k_{eff}^b is the effective ionization rate coefficient in the pure buffer gas, m_e is the electron mass, $\sigma_a(\varepsilon)$ are the attachment

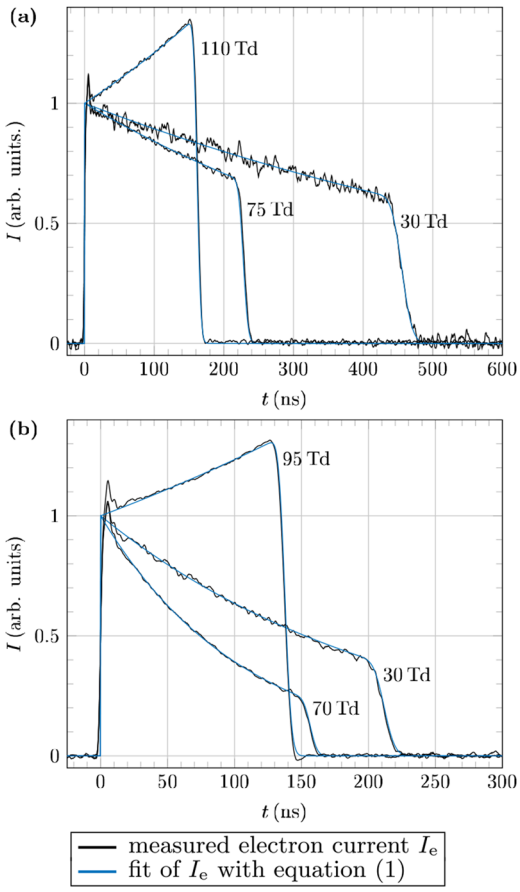

FIG. 1. Measured and fitted electron current for an electrode spacing of 19 mm, at a total pressure of 10 kPa (a) in a mixture of 0.26% HFPO in N_2, for different ratios of the electric field to the gas density: E/N = 30, 75, and 110 Td, (b) in a mixture of 0.48% HFPO in CO_2, for different ratios of the electric field to the gas density: E/N = 30, 70, and 95 Td. The currents were rescaled to the same amplitude at t = 0 for easier comparison, and original amplitudes were ranging from 8 to 35 μA.

cross sections of the attaching gas, and $f(E/N, \varepsilon)$ is the electron energy distribution function (EEDF) in the buffer gas. The underlying assumption of this method is that the EEDF in the gas mixture is the same as in the pure buffer gas.

For the presently considered buffer gases N_2 and CO_2, complete sets of electron scattering cross sections are available, for instance, via the LXcat project.[22] In the present work, the cross section set of Biagi[23] is used for N_2 and that of Phelps[24] is used for CO_2. The electron swarm parameters and electron energy distribution function of these gases are calculated by solving the Boltzmann equation in the two-term approximation using the solver Bolsig+.[25]

III. RESULTS

A. Beam experiment

Figure 2 shows the cumulative negative ion mass spectrum following the electron attachment to HFPO in the energy range 0–7 eV. A rich fragmentation pattern can be seen, with the dominant fragment ion being F^-. The electron attachment is completely dissociative, and the parent anion $C_3F_6O^-$ has not been detected. Figure 3 shows the partial DEA cross sections. The shapes of individual ion yields differ only slightly; all

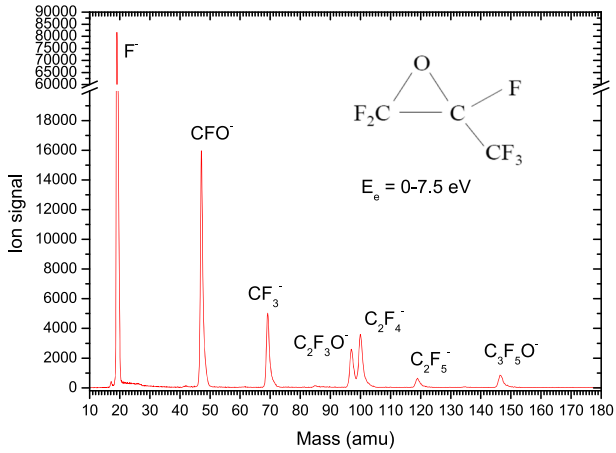

FIG. 2. Cumulative negative ion mass spectrum of HFPO for the electron energies 0-7 eV. The spectrum is obtained a sum of 70 mass spectra taken at different electron energies with the step of 0.1 eV.

the cross sections show one broad band with the maximum between 2 and 3 eV. Figure 6 shows the total beam cross section σ_{Beam} obtained as a sum of all the partial cross sections from Fig. 3.

B. Swarm experiment

1. Electron rate and transport coefficients

The effective ionization rate coefficient k_{eff}, the electron drift velocity w_e, and the longitudinal electron diffusion

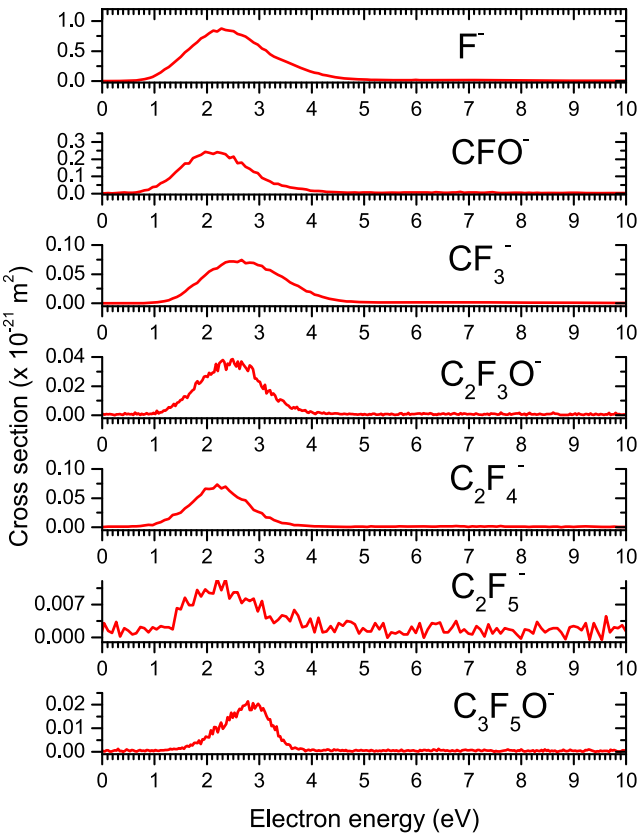

FIG. 3. Partial dissociative electron attachment cross sections recorded in the beam experiment.

coefficient ND_L obtained in the mixture of 0.26% HFPO in N_2 are shown in Fig. 4 and the same quantities obtained in the mixture of 0.48% HFPO in CO_2 are shown in Fig. 5. These data are made available in the online database ETHZ of the LXcat project.[26] The measured values of k_{eff}, w_e, and ND_L in pure N_2 and in pure CO_2 are in excellent agreement with the same quantities calculated with the solver Bolsig+ using the cross section sets of Biagi and Phelps, respectively. The measured values of k_{eff} in the HFPO/N_2 and HFPO/CO_2 mixtures are lower than in N_2 and CO_2 due to electron attachment to HFPO. By contrast, the measured values of w_e and ND_L in the HFPO/N_2 and HFPO/CO_2 mixtures are essentially the same as in N_2 and CO_2. This confirms the important above-mentioned assumption about the same EEDF in the mixture and in the pure buffer gas.

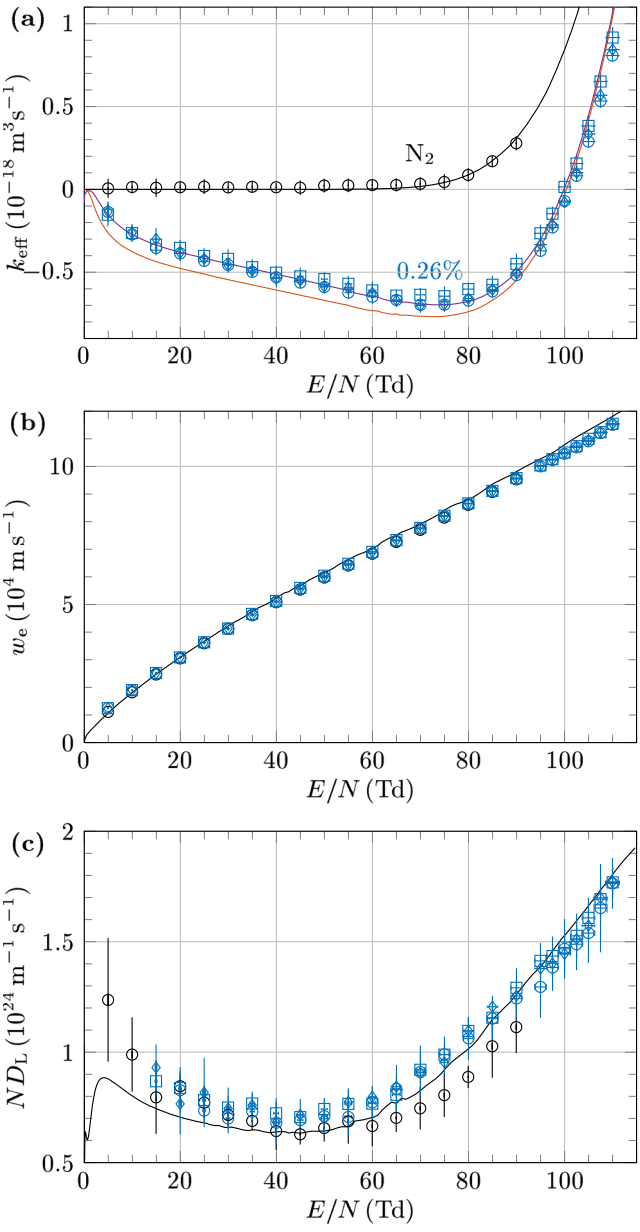

FIG. 4. (a) Effective ionization rate coefficient, (b) drift velocity, and (c) diffusion coefficient as functions of E/N in pure N_2 and in the mixture of 0.26% HFPO in N_2. The data of pure N_2 are in black, whereas the data of the HFPO/N_2 mixture are in color. Measurements are plotted with markers, the marker shape indicating the total gas pressure during the measurement: □ 2 kPa, ◇ 4 kPa, ○ 6 kPa, ◁ 8 kPa, and ▽ 10 kPa. Calculations are plotted with lines: black line—k_{eff}, w_e, and ND_L in N_2 calculated using Biagi's data,[23] red line—k_{eff}^{Beam}, purple line—k_{eff}^{Swarm}.

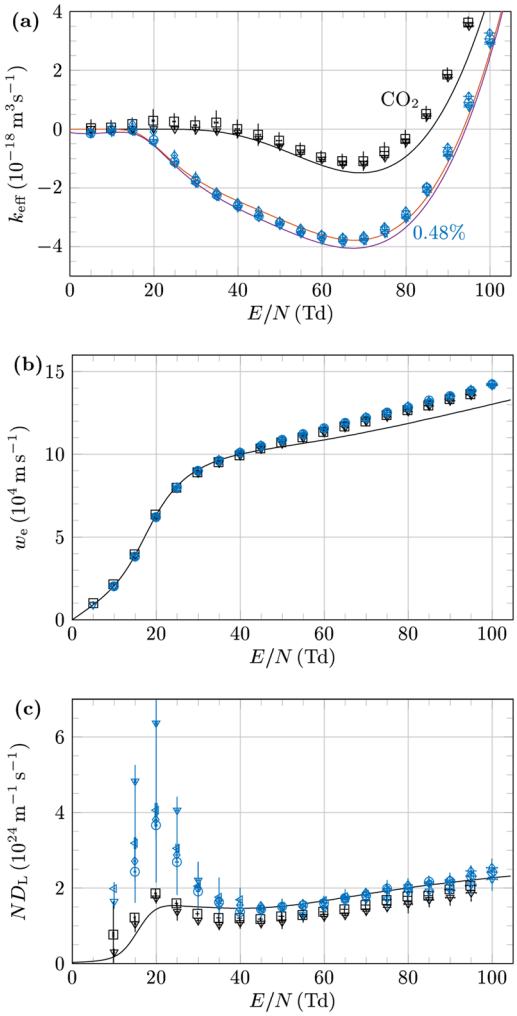

FIG. 5. (a) Effective ionization rate coefficient, (b) drift velocity, and (c) diffusion coefficient as functions of E/N in pure CO_2 and in the mixture of 0.26% HFPO in CO_2. The data of pure CO_2 are in black, whereas the data of the HFPO/CO_2 mixture are in color. Measurements are plotted with markers, the marker shape indicating the total gas pressure during the measurement: □ 2 kPa, ◇ 4 kPa, ○ 6 kPa, ◁ 8 kPa, and ▽ 10 kPa. Calculations are plotted with lines: black line—k_{eff}, w_e, and ND_L in CO_2 calculated using Phelps' data,[24] red line—k_{eff}^{Beam}, purple line—k_{eff}^{Swarm}.

2. Electron attachment cross section

The measured effective ionization rate coefficient k_{eff} in the HFPO/N_2 and HFPO/CO_2 mixtures is used to obtain an estimation σ_{Swarm} of the total electron attachment cross section of HFPO with the linear inversion method described by Rabie *et al.*[21] The estimation σ_{Swarm} is shown in Fig. 6 and compared to the total electron attachment cross section σ_{Beam} measured with the crossed-beam experiment. To verify the consistency of σ_{Swarm} and σ_{Beam} with the measurements of k_{eff} in the swarm experiment, k_{eff}^{Swarm} and k_{eff}^{Beam} are calculated from σ_{Swarm} and σ_{Beam} using Eq. (3) and plotted in Figs. 4(a) and 5(a). k_{eff}^{Swarm} and k_{eff}^{Beam} are in good agreement with the measured values of k_{eff} in the HFPO/N_2 and HFPO/CO_2 mixtures.

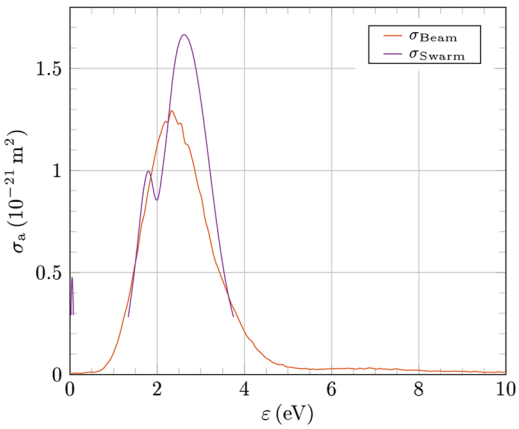

FIG. 6. Total electron attachment cross section of HFPO from the beam experiment σ_{Beam} and from the swarm experiment (linear inversion) σ_{Swarm}.

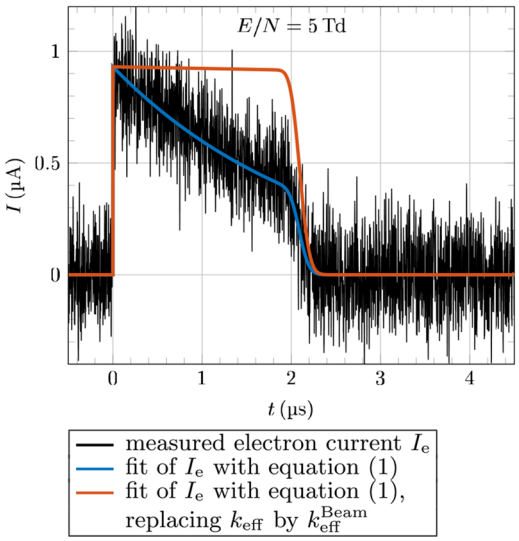

FIG. 7. Measured and modeled electron current in a mixture of 0.48% HFPO in CO_2, at a pressure of 10 kPa, for an electrode spacing of 19 mm and for E/N = 5 Td.

A particular point of interest is that σ_{Swarm} suggests a small attachment peak towards 0 eV which is not present in σ_{Beam}. It seems that this peak is not an artifact but is really reflecting the electron attachment measured in the swarm experiment at low E/N. To illustrate this point, the current measured at E/N = 5 Td in the HFPO/CO_2 mixture is shown in Fig. 7. It shows an exponential decrease in time due to electron attachment, whereas using the effective ionization coefficient $k_{\mathrm{eff}}^{\mathrm{Beam}}$ calculated with the beam experiment very little electron attachment is expected, which corresponds to a flat current profile in Fig. 7.

IV. DISCUSSION

A. Comparison of the two methods

The total attachment cross sections σ_{Beam} and σ_{Swarm} shown in Fig. 6 are in very good agreement. One should bear in mind that the unfolded cross section σ_{Swarm} is a result of linear inversion: a complex mathematical procedure where the best fit to the measured swarm effective ionization coefficient is sought over a wide range of reduced electric fields. It should thus be viewed as an estimate of the cross section energy range and magnitude, especially due to its sensitivity to the EEDF in Eq. (3), which in turn depends on the chosen cross section sets for the buffer gases. For example, the fine structure (dip) at 2 eV is certainly a mathematical artifact of the inversion procedure. A good indication of the consistency of the beam and swarm data is the effective ionization rate coefficients evaluated from Eq. (3) shown in Figs. 4 and 5 as red lines. Even though the agreement with the data is not as perfect as in the case of the swarm-unfolded cross section, the magnitude and general trend of the rate coefficients are reproduced very well.

The present agreement is in contrast to a number of different gases, where the swarm cross sections are consistently higher than those obtained at single-collision conditions, sometimes even by several orders of magnitude.[12,13,27,28] The origin of this is three-body processes. The electron attachment proceeds via formation of transient anions (resonances).[29] At single collision conditions, these release the excess energy either via dissociation, forming stable anions, or via electron detachment (autodetachment). Their lifetimes vary from the time scale typical for vibrational motion (femto- or picoseconds) to much longer time scales (micro to milliseconds) for transient anions where the excess energy can be redistributed among the internal degrees of freedom for such a long time.[14] If, in a higher-pressure environment, during its lifetime the transient anion collides with a buffer gas molecule, the excess energy can be carried away in the collision. Thus, the anion can be stabilized and the autodetachment is suppressed. Such stabilization can be surprisingly effective[30] and lead to higher swarm electron attachment cross sections. The present very good agreement of the beam and swarm data suggests a very short lifetime of the transient HFPO anions (prompt dissociation).

An exception is the small peak close to 0 eV in the swarm cross section. No such ions have been detected in the beam experiment. The detection window of the latter requires the lifetime of the ion to be longer than 1 μs. The mean time between collisions in the swarm experiment is in the order of nanoseconds; so, if there is a transient $HFPO^-$ anion with the natural lifetime between the ns and μs range formed at 0 eV, it could, in principle, lead to this discrepancy. However, almost no pressure dependence is observed in the value of the swarm ionization rate at low reduced field values. An alternative explanation for the weak 0 eV peak might be the presence of the impurity in the sample. HFPO may rearrange to hexafluoroacetone (HFA), with the structure $CF_3C(=O)CF_3$, over a few months inside its container.[31] Since the HFPO samples used in the beam and swarm experiments were procured from different vendors, and at different times, they may have different levels of hexafluoroacetone (HFA) impurity. Electron attachment to HFA was studied by Illenberger *et al.*;[32] it proceeds dominantly by parent ion attachment at 0 eV. Therefore, the HFA impurity could cause the small attachment peak at thermal electron energies suggested by the swarm measurements.

B. Fragmentation pattern and DEA mechanism

In order to elucidate the mechanism of the bond-breaking process, we have performed quantum chemical calculations of the threshold energies E_{th} for the observed fragmentation channels (Table I). The energies were calculated at the B3LYP/aug-cc-pVTZ level. They are obtained as differences between the total energies (electronic plus zero-point energies) of the products and reactants. A few observations can be made based on these values.

TABLE I. B3LYP/aug-cc-pVTZ threshold energies for individual DEA fragmentation channels. The inset pictures show molecules or fragments where the structure is not obvious from the summation formula.

Products		m/z	E_{th} (eV)
F_i^- i=a,b,c,d,e,f	$+ C_3F_5O$	19	$1.56 \rightarrow F^-_{(a,\,b)}$ $1.53 \rightarrow F^-_{(c,\,d,\,e)}$ $1.30 \rightarrow F^-_{(f)}$ 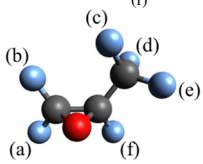
CFO^-	$+ C_2F_5$ 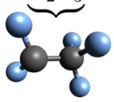	47	–0.25
CFO^-	$+ C_2F_4 + F$ 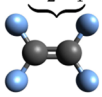	47	2.75
CFO^-	$+ C_2F_4 + F$ 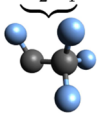	47	4.53
CF_3^-	$+ C_2F_3O$ 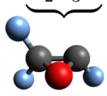	69	1.94
$C_2F_3O^-$	$+ CF_3$	97	1.27
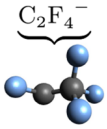	$+ CF_2O$	100	–0.16
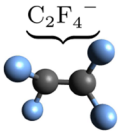	$+ CF_2O$	100	0.30
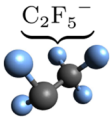	$+ CFO$	119	0.24
$C_3F_5O^-$	$+ F_i$	147	$2.54 \rightarrow F_{(a)}$ $2.58 \rightarrow F_{(b)}$ $3.07 \rightarrow F_{(c,d,e)}$ $2.16 \rightarrow F_{(f)}$

As to the dominant F^- anion, when the fluorine is cleaved from the (f) position, the threshold is by some 0.2 eV lower than when it is cleaved from the other five possible positions. The experimental band does not have a sharp onset and is rising only slowly between 1 and 2 eV. This does not allow for an unambiguous determination of the fragmentation site. However, due to the energetic reasons, we presume that most of the observed F^- fragments originate from the (f) site.

The second strongest fragment, CFO^-, is certainly produced by two-body breakup, creating a C_2F_5 radical as the neutral counterpart, since the channels involving the production of the F-atom have computed thresholds considerably higher than the onset of the experimental band. This fragment and one more fragment, $C_2F_4^-$, show a somewhat surprising effect: in spite of the fact that the fragmentation channel is exothermic, they do not show peaks close to 0 eV. This suggests that there is no anion state below or close to the neutral potential energy surface at the geometry of the neutral and that the lowest temporary anion state (resonance) lies between 2 and 3 eV, the one that is visible in the cross sections of all the fragments. The only fragment with somewhat different ion yield shape is the defluorinated parent ion $C_3F_5O^-$, for which the DEA band is cut off by the rather high energy threshold for this process.

We have additionally calculated with the same method the threshold energies for the (not-observed) channels that would hypothetically form the CF_2 anion or radical, which dominates the reactive chemistry in HFPO plasmas,[3,4,6]

$$e^- + \mathrm{HFPO} \rightarrow CF_2^- + C_2F_4O, E_{th} = 0.47\ \mathrm{eV}, \quad (4)$$

$$e^- + \mathrm{HFPO} \rightarrow CF_2 + C_2F_4O^-, E_{th} = 0.18\ \mathrm{eV}. \quad (5)$$

Both of these channels have threshold energies well below the energy of the dominant resonance, but none of the fragments have been experimentally detected. As shown below, this confirms our hypothesis about DEA happening on a very short time scale. Additionally, it rules out the DEA as a possible source of the CF_2 radical in plasmas. Since the positive ionization mass spectrum[33] of HFPO does not contain the $C_2F_4O^+$ fragment, which would be a charged counterpart of CF_2 in the dissociative ionization, we conclude that the most probable elementary process leading to its production is the electron-induced neutral dissociation. This process can lead to very different reaction channels than DEA or the positive ionization.[34,35]

Several findings outlined above suggest that the DEA mechanism is a vertical electron attachment followed by a prompt dissociation, rather than an internal vibrational redistribution of the excess energy and statistical dissociation. These findings are the absence of the collisional stabilization in the swarm experiment and the fact that the relative abundances of the fragments are not at all correlated with the asymptotic energetics. The reaction outcome is thus given by the dissociative direction of the involved resonant potential energy surface at the geometry of the vertical attachment.[36] The involved resonance can be identified using an empirical relation between the unoccupied molecular orbitals and the corresponding resonances which are formed by temporarily

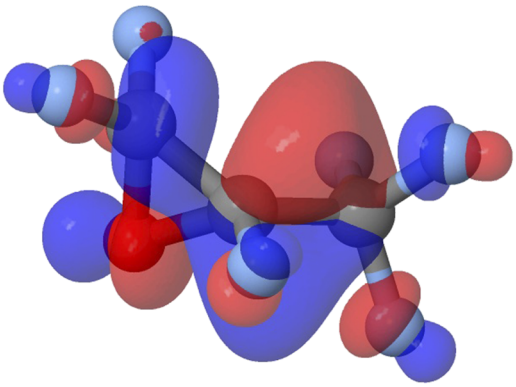

FIG. 8. The lowest unoccupied molecular orbital (LUMO) of HFPO.

occupying these orbitals.[37] Chen and Gallup[38] developed a scaling formula which relates these two energies. This scaling [E_{res} = (E_{MO} − 2.33 eV)/1.31] predicts that the lowest unoccupied orbital of HFPO (E_{MO} = 5.8 eV), shown in Fig. 8, will lead to a resonance at 2.65 eV. This estimate is in very good agreement with the maxima of the experimental DEA bands, and we thus conclude that this is the transient anion state mediating the electron attachment. The dominant contribution to the LUMO comes from the C–F bond antibonding σ^* orbitals. Consequently, it has a number of nodal planes crossing the C–F bonds which agrees with the fact that the direct cleavage of this bond is the main fragmentation channel.

V. CONCLUSIONS

In conclusion, we have characterized the electron attachment to HFPO using two experimental approaches. The data taken at single collision conditions are in very good agreement with the data taken at pressures five orders of magnitude higher in the swarm experiment. The electron attachment is completely fragmentative with the dominant fragment ion being F^-. Only one transient anion state is involved in the attachment, which corresponds to the temporary occupation of HFPO's LUMO and leads to one prominent band in all partial cross sections. The dissociation of this transient state is prompt and occurs on the time scale shorter than nanoseconds.

ACKNOWLEDGMENTS

This work is part of the Project No. 17-04844S of the Czech Science Foundation. A. Chachereau and C. M. Franck acknowledge financial support from GE Grid (Switzerland) GmbH, Pfiffner Technologie AG, ABB Switzerland Ltd., and Siemens AG. We thank D. Kollárová, Prague, for her help in carrying out some of the experiments.

[1] G. Siegemund, W. Schwertfeger, A. Feiring, B. Smart, F. Behr, H. Vogel, and B. McKusick, *Fluorine Compounds, Organic. Ullmann's Encyclopedia of Industrial Chemistry* (Wiley-VCH, Weinheim, 2018).
[2] M. Ng, D. K. Mok, J. M. Dyke, and E. P. Lee, J. Fluorine Chem. **159**, 29 (2014).
[3] B. A. Cruden, K. K. Gleason, and H. H. Sawin, J. Appl. Phys. **89**, 915 (2001).
[4] A. Carletto and J. P. S. Badyal, J. Phys. Commun. **1**, 055024 (2017).
[5] A. Milella, F. Palumbo, and R. d'Agostino, in *Advanced Plasma Technology*, edited by R. d'Agostino, P. Favia, Y. Kawai, H. Ikegami, N. Sato, and F. Arefi-Khonsari (WILEY-VCH Verlag GmbH, Weinheim, 2008), pp. 175–195.
[6] B. A. Cruden, K. K. Gleason, and H. H. Sawin, J. Appl. Phys. **91**, 9547 (2002).
[7] M. Dicko, G. Belaribi-Boukais, C. Coquelet, A. Valtz, F. Brahim Belaribi, P. Naidoo, and D. Ramjugernath, Ind. Eng. Chem. Res. **50**, 4761 (2011).
[8] G. Myhre, D. Shindell, F.-M. Bréon, W. Collins, J. Fuglestvedt, J. Huang, D. Koch, J.-F. Lamarque, D. Lee, B. Mendoza *et al.*, in *Climate Change 2013: The Physical Science Basis. Contribution of Working Group I to the Fifth Assessment Report of the Intergovernmental Panel on Climate Change*, edited by T. Stocker, D. Qin, G.-K. Plattner, M. Tignor, S. Allen, J. Boschung, A. Nauels, Y. Xia, V. Bex, and P. Midgley (Cambridge University Press, Cambridge, United Kingdom; New York, NY, USA, 2013), pp. 659–740, ISBN: 978-1-107-66182-0.
[9] See https://echa.europa.eu/registration-dossier/-/registered-dossier/5721/5/7 for European Chemicals Agency (ECHA); accessed 11 August 2017.
[10] *Environmental Issues in the Electronics/Semiconductor Industries and Electrochemicl/Photochemical Methods for Pollution Abatement*, edited by C. R. Simpson, L. Mendicino, K. Rajeshwar, and J. M. Fenton (The Electrochemical Society, 1998), Vol. 98-5, ISBN: 1-56677-199-4.
[11] D. Nalewajek, A. J. Poss, and C. L. Cantlon, "Fumigant compositions and methods based on hexafluoropropylene oxide (HFPO)," patent WO/2018/057553, URL: http://www.freepatentsonline.com/y2018/0077932.html (2018).
[12] *Electron-Molecule Interactions and Their Applications*, edited by L. G. Christophorou (Academic Press, Orlando, 1984), Vol. 1.
[13] A. Chachereau, J. Fedor, R. Janečková, J. Kočišek, M. Rabie, and C. M. Franck, J. Phys. D: Appl. Phys. **49**, 375201 (2016).
[14] J. Kočišek, R. Janečková, and J. Fedor, J. Chem. Phys. **148**, 074303 (2018).
[15] O. May, J. Fedor, B. C. Ibănescu, and M. Allan, Phys. Rev. A **77**, 040701(R) (2008).
[16] O. May, J. Fedor, and M. Allan, Phys. Rev. A **80**, 012706 (2009).
[17] R. Janečková, D. Kubala, O. May, J. Fedor, and M. Allan, Phys. Rev. Lett. **111**, 213201 (2013).
[18] M. Stepanović, Y. Pariat, and M. Allan, J. Chem. Phys. **110**, 11376 (1999).
[19] D. A. Dahl, T. H. Teich, and C. M. Franck, J. Phys. D: Appl. Phys. **45**, 485201 (2012).
[20] A. Chachereau, M. Rabie, and C. M. Franck, Plasma Sources Sci. Technol. **25**, 045005 (2016).
[21] M. Rabie, P. Haefliger, A. Chachereau, and C. M. Franck, J. Phys. D: Appl. Phys. **48**, 075201 (2015).
[22] L. C. Pitchford, L. L. Alves, K. Bartschat, S. F. Biagi, M.-C. Bordage, I. Bray, C. E. Brion, M. J. Brunger, L. Campbell, A. Chachereau *et al.*, Plasma Processes Polym. **14**, 1600098 (2017).
[23] See www.lxcat.net/Biagi for Biagi database on LXcat, data extracted from the Fortran program MAGBOLTZ of S.F. Biagi, versions 8.9 and after, data retrieved on April 19, 2017.
[24] See www.lxcat.net/Phelps for Phelps database on LXcat, data retrieved on June 27, 2014.
[25] G. Hagelaar and L. Pitchford, Plasma Sources Sci. Technol. **14**, 722 (2005).
[26] See www.lxcat.net/ETHZ for ETHZ database on LXcat.
[27] K. Graupner, S. A. Haughey, T. A. Field, C. A. Mayhew, T. H. Hoffmann, O. May, J. Fedor, M. Allan, I. I. Fabrikant, E. Illenberger *et al.*, J. Phys. Chem. A **114**, 1474 (2010).
[28] M. J. E. Casey, J. de Urquijo, L. N. S. Loli, D. G. Cocks, G. J. Boyle, D. B. Jones, M. J. Brunger, and R. D. White, J. Chem. Phys. **147**, 195103 (2017).
[29] I. I. Fabrikant, S. Eden, N. J. Mason, and J. Fedor, Adv. At., Mol., Opt. Phys. **66**, 545 (2017).
[30] M. Zawadzki, M. Ranković, J. Kočišek, and J. Fedor, Phys. Chem. Chem. Phys. **20**, 6838 (2018).
[31] See http://www2.dupont.com/FluoroIntermediates/en_US/assets/downloads/k05132.pdf for DuPont HFPO: Properties, Uses, Storage, and Handling.
[32] E. Illenberger and M. C. Meinke, Int. J. Mass Spectrom. **365-366**, 80 (2014).
[33] See https://chemdata.nist.gov/ for NIST Mass Spectrometry Data Center.
[34] M. Zlatar, M. Allan, and J. Fedor, J. Phys. Chem. C **120**, 10667 (2016).
[35] M. Allan, M. Lacko, P. Papp, Š. Matejčík, M. Zlatar, I. I. Fabrikant, J. Kočišek, and J. Fedor, Phys. Chem. Chem. Phys. **20**, 11692 (2018).
[36] R. Janečková, O. May, A. R. Milosavljević, and J. Fedor, Int. J. Mass Spec. **365-366**, 163 (2014).
[37] M. Allan, O. May, J. Fedor, B. C. Ibănescu, and L. Andric, Phys. Rev. A **83**, 052701 (2011).
[38] D. Chen and G. A. Gallup, J. Chem. Phys. **93**, 8893 (1990).